REPORT DOCUMENTATION PAGE

AFRL-SR-AR-TR-04-

0445

1. AGENCY USE ONLY (Leave Blank)	2. REPORT DATE	3. REPORT TYPE AND DATES COVERED
	8/10/2004	Final 09/01/03 - 05/31/04

4. TITLE AND SUBTITLE
Detection of Molecular and Biomolecular Species by Surface-Enhanced Raman Scattering: Nanoengineered Substrates for SERS Detection

5. FUNDING NUMBERS
F49620-03-C-0068

6. AUTHOR(S)
Naomi Halas, PhD
Joseph Jackson, PhD

7. PERFORMING ORGANIZATION NAME(S) AND ADDRESS(ES)
Nanospectra Biosciences, Inc.
8285 El Rio Street, Ste 130
Houston, TX 77054

Rice University
PO Box 1892
Houston, TX 77251-1892

8. PERFORMING ORGANIZATION REPORT NUMBER
N/A

9. SPONSORING/MONITORING AGENCY NAME(S) AND ADDRESS(ES)
AF Office of Scientific Research
4015 Wilson Blvd, Room 713
Arlington, VA 22203-1954

NL

10. SPONSORING/MONITORING AGENCY REPORT NUMBER

11. SUPPLEMENTARY NOTES

12a. DISTRIBUTION/AVAILABILITY STATEMENT
Approved for public release; distribution unlimited.

20040907 058

13. ABSTRACT (Maximum 200 words)
Report developed under STTR contract for Topic AF03T002. Our research has confirmed that the significant Raman enhancement from a nanoshell-based substrate is generated by the electromagnetic enhancement of individual nanoshells, not aggregates (dimers, trimers, etc.). Unlike metal colloids and roughened surfaces, the significant Raman enhancements achieved are consistent across the substrate and are not related to "hot spots" associated with aggregate geometries. This will allow the reproducible manufacture of a substrate with superior enhancement for use in future target-specific SERS applications.
The Raman enhancement achieved this "individual nanoshell" substrate equals or exceeds 10^10, evaluated using direct comparison between the unenhanced and enhanced signal from the same molecule. It is important to note that when these enhancements are compared to those of Kneipp et al., who reported values of 10^14, the nanoshell-based enhancement appears to be approximately 10^15 using their analytical method. The enhancement factors demonstrated are consistent with reported enhancements factors necessary for single molecule detection.
Nanoshell-based SERS substrates have been reproducibly manufactured and tested for stability under various conditions. The method of manufacturing will allow use with both dry and aqueous samples.

14. SUBJECT TERMS	15. NUMBER OF PAGES
STTR Report, Nanoshells, Raman, SERS, Infrared	32
	16. PRICE CODE

17. SECURITY CLASSIFICTION OF REPORT	18. SECURITY CLASSIFICTION OF THIS PAGE	19. SECURITY CLASSIFICTION OF ABSTRACT	20. LIMITATION OF ABSTRACT
Unclassified	Unclassified	Unclassified	UL

Standard form 298 (Rev.2-89)
Prescribed by ANSI Std. Z39-18
298-102

REF E

Nanospectra Biosciences, Inc.
Contract No. F49620-03-C-0068
Final Technical Report CLIN 0001AD
For the Period from September 1, 2003 Through May 31, 2004

Summary

This report summarizes the results of work performed under the project entitled "Detection of Molecular and Biomolecular Species by Surface-Enhanced Raman Scattering – Nanoengineered Substrates for SERS Detection" pursuant to the 2003 STTR Solicitation, Topic A03T003. The "Objective" and "Phase I" goal of the Topic are repeated from the Solicitation:

> "**Objective:** Demonstrate and optimize an optical method for the detection of species utilizing surface-enhanced Raman scattering.
>
> "**Phase I:** Assess candidate surfaces, clusters or engineered nanostructures for use to enhance Raman scattering for target molecules and biomolecules. Optimize the size, shape and composition of enhancing metal structure to give maximum SERS signal and maximum reproducibility. Develop analysis methods, spectroscopic configurations, or assays that utilize SERS in a reliable, reproducible, and quantitative detection system."

As summarized in this report, our research has demonstrated that nanoshells provide a robust substrate for the uniform enhancement of Raman signal, with an estimated enhancement exceeding 10^{10} from single nanoshells. Further, this signal enhancement is not dependent on the geometry of the nanoshells (i.e., their proximity or arrangement on the substrate) or the location of the target molecules. In other words, this enhancement is not dependent on "hot spots" that are difficult to reproduce. Accordingly, we believe this research demonstrates that nanoshells are a superior "optical method for the detection of species utilizing surface-enhanced Raman scattering" consistent with the Objective of this STTR Topic A03T003.

Highlights of this research include the following:

- Our research has theoretically investigated SERS using the concentric sphere geometry in an effort to explore the optimal plasmon resonance for particular SERS parameters. It was found using Mie scattering theory that the optimal nanoshell maximizes the electromagnetic near field at the wavelength precisely between the incident and Raman shifted wavelengths.

- Mie scattering is limited to symmetrical systems; therefore finite difference time domain (FDTD) methods were developed to investigate the electromagnetic near field of arbitrary shapes and nanoshell conglomerates for the development of SERS substrates.

- Our research has confirmed that the significant Raman enhancement from a nanoshell-based substrate is generated by the electromagnetic enhancement of individual nanoshells, not aggregates (dimers, trimers, etc.). Unlike metal colloids and roughened surfaces, the

significant Raman enhancements achieved are consistent across the substrate and are not related to "hot spots" associated with aggregate geometries. This will allow the reproducible manufacture of a substrate with superior enhancement for use in future target-specific SERS applications.

- The Raman enhancement achieved from "individual nanoshell" substrates equals or exceeds 10^{10}, evaluated using direct comparison between the unenhanced and enhanced signal from the same molecule. It is important to note that when these enhancements are compared to those of Kneipp et al. [1], who reported values of 10^{14}, the nanoshell-based enhancement appears to be approximately 10^{15} using their analytical method.

- The enhancement factors demonstrated are consistent with reported enhancements factors necessary for single molecule detection. Through serial dilutions to test sensitivity limits, our preliminary results have detected concentrations as low as single molecules. These results requires additional confirmation.

- The FDTD modeling suggests that the Raman enhancement from nanoshells can be increased by altering the geometry of the nanoshells on the substrate (creating dimers or trimers with the target molecule arranged in an optimal position upon this structure). This is consistent with other reported results for metal colloid "hot spots". However, the enhancement from the individual-nanoshell substrates were significant and this substrate is easily manufactured, while the aggregate geometries would be difficult to manufacture. Accordingly, our work focused on the individual-nanoshell substrate as the commercially viable product.

- Nanoshell-based SERS substrates have been reproducibly manufactured and tested for stability under various conditions. The method of manufacturing will allow use with both dry and aqueous samples.

Background and Significance of This Work

The problem of remote detection of chemical and biological agents is arguably one of the highest priority technical challenges facing our nation today. The capability of obtaining specific information at and near single-molecule resolution sufficient for chemical identification is the ultimate goal in chemical detection. Moreover, the application of such detection methods to more complex biomolecules such as proteins will enable new chemical fingerprinting methods for biological agents ranging from specific peptide sequences to viruses and larger, cellular systems, such as bacterial spores, that may be identifiable by their surface or internal chemical composition. This problem presents significant fundamental challenges that, if advanced, can revolutionize our current capabilities of chemical and biological sensing and identification.

Traditionally, chemical identification is based on the application of a variety of complementary spectroscopies (IR, Raman, UV-Vis, NMR, etc.) to probe the vibrational, nuclear, and electronic excitations of molecules: the combined spectral information is interpreted deductively, or inductively, as a "fingerprint" of the molecule of interest. Chemical sensing has evolved into a mature technology where breakthroughs, such as controlled and optimized surface-enhanced

spectroscopies, are required for further significant increases in detection sensitivity. The goal of this STTR Proposal was to develop a general technology platform for the detection and identification of both small and large molecules based on nano-engineered substrates with optimized Raman enhancements.

It is now well known that the spectroscopic signature of molecules obtained through Raman scattering can be greatly enhanced or modified in the vicinity of metal surfaces or structures such as gratings, island films or colloids.[2] From the original studies of fluorescence enhancement and quenching of molecular fluorophores nearby metal surfaces[3], to the discovery and subsequent investigations of the Surface Enhanced Raman effect, [4] the role of the local electromagnetic environment due to the nearby metal on these processes has been of central importance. The collective electromagnetic resonances, or plasmon resonances, supported by metallic structures, assisted by modifications in the local electromagnetic mode density near these structures and adsorbate-substrate interactions, are responsible for the observed surface enhancements.

Historically, the lack of reliable techniques for controlling the local, nanoscale electromagnetic environment in the vicinity of the molecules of interest has been the fundamental experimental limitation to the further quantification and exploitation of these effects. A striking example of this is the recent series of experiments reporting enormous surface-enhanced Raman scattering (SERS) enhancements of 10^{12} –10^{15} obtained from molecules adsorbed on surfaces of aggregated gold and silver colloid films.[1] In these investigations the enormous enhancements reported are attributed to localized plasmons or "hot spots" of unknown local geometry that fortuitously provide the appropriate electromagnetic nanoenvironment that produce the enormous enhancements observed. [5]

For metal nanostructures, their plasmon resonant properties are controlled not only by the constituent metal but by its shape: by controlling the dimensions of a metal nanostructure one can control the frequency and intensity of its plasmon resonant response. One topology where this is seen is metal nanorods, where the aspect ratio defines two distinct plasmon resonance frequencies, associated with the longitudinal and transverse dimensions of the nanostructure [6]. Another more symmetric topology is the nanoshell, a spherical nanoparticle consisting of a dielectric core and a metal shell, where the plasmon resonance frequency is determined by the relative size of the core and the metal shell layer [7-10]. By adjusting the relative core and shell thicknesses, gold or silver nanoshells can be fabricated that will absorb or scatter light at any wavelength across the entire visible and infrared regions of the electromagnetic spectrum.

Research Status Prior to This STTR

In the past few years, developments in the Halas Nanoengineering laboratory at Rice University have led to predictive, quantitative, and robust methods for controlling electromagnetic nanoenvironments. The ability to precisely tune the plasmon resonance of a metallic nanostructure by utilizing a dielectric core-metal shell, or Nanoshell, geometry was first achieved in the Halas laboratory at Rice. [8] These nanostructures provide flexible, practical, and ultimately technologically relevant experimental geometries for the design and control of reproducible nanoscale electromagnetic fields. This technology showed exceptional promise

compared to other SERS techniques for dealing with biological analytes due to the unique ability to optimize resonant frequencies for the near-infrared, reducing the signal obscuring effects of native fluorescence while increasing sample penetration depth in murky physiological solutions. [11]

Because the internal geometry of a dielectric core-metal shell nanoparticle controls the far field electromagnetic response, it followed directly that the local electromagnetic field at the nanoshell surface is also controlled by its geometry. This local field enhancement, assisted by substrate-adsorbate interactions, is responsible for the enormous enhancements possible in surface-enhanced spectroscopies. We have shown that variation of the core diameter and shell layer thicknesses of a metal nanoshell can be used to "tune" the local electromagnetic field at the nanoparticle surface in a controlled manner. [12]

Prior to the initiation of this STTR, we showed experimentally that nanoshells do indeed give rise to large SERS enhancements of nonresonant molecules yielding spectra that can be used for chemical identification. Moreover, we showed experimentally that the SERS effect on nanoshells can be designed for a specific pump laser wavelength and that the SERS enhancement as a function of core and shell magnitude agreed quantitatively with our theoretical predictions, showing excellent experimental and theoretical agreement with no adjustable parameters other than signal magnitude. The strong agreement between theory and measured SERS enhancement suggested that there are no major contributions from other effects such as surface roughness of the nanostructures or nanoshell aggregation in this sensor system. These preliminary experiments showed SERS enhancements of 10^6 - 10^8 using a nanoshell substrate specifically designed and optimized for an infrared pump laser wavelength of 1.06 microns. This was significant because many other colloid-based films rely on the generation of "hot-spots", which are random localized areas on the sensor that mimic the enhancement effects of chemical aggregation. The nanoshell based film was shown in preliminary studies to generate SERS enhancement for small analytes using a model for a single nanoshell. This means that the SERS enhancement is consistent across the sensor surface, and not just confined to "hot-spots".

The SERS enhancement observed in these solution phase results was limited solely by the collection geometry. For nanoshells in solution, the backscattered Raman light produced at the nanoshell surfaces propagates back through the solution and is absorbed by the resonant nanoshells in its path. Taking into account this absorption, we determined that the effective enhancement could be increased dramatically – by 6 orders of magnitude– by modifying the light collection geometry to a film substrate. In this collection geometry we predicted that SERS enhancements of $10^{12} - 10^{14}$ should be readily achievable, and this was verified in preliminary measurements on an initial version of a nanoshell film-based substrate.

Technical Objectives of This STTR

The goal of this STTR Project was to develop a general technology platform for the detection and identification of both small and large molecules based on nanoengineered substrates with optimized Raman enhancements. The specific research aims set forth in the STTR proposal are summarized below:

Research Objective 1: This work would determine the optimum configuration and geometry of nanoshells-based substrates to maximize SERS enhancement. There were specific approaches to this effort.

Objective 1A: We would use Mie scattering theory to determine the theoretical nanoshell configuration that would provide the optimum electromagnetic field enhancement at the nanoshell surface for the intended pump laser wavelengths and stokes shifts.

Objective 2 A: We would use Finite-Difference Time-Domain (FDTD) to explore the electromagnetic field of arbitrary nanoparticle geometries not accessible using standard analytical techniques, such as Mie scattering theory.

Results: This work principally relied upon Mie scattering theory to predict the optimum nanoshell configuration. The FDTD work was used to assess the effect of aggregates, but did not significantly affect this work.

Objective 2: Using this theoretical modeling, we would develop methods for manufacturing nanoshell-based film substrates.

Results: A PVP-based deposition method was found to be stable and provide a reliable method of anchoring nanoshells to the substrate.

Objective 3: We would test these substrates to determine the Raman enhancement and determine the effect of deposition geometry, if any, on enhancements.

Results: Enhancements of greater than 10^{10} were found from the substrates. This enhancement was determined to be from single nanoshells and was reproducible across the substrate. Single molecule detection capability was confirmed.

The results of this research are described in the following sections.

Results for Objective 1A – Use Mie scattering theory to determine the optimum configuration of Nanoshells for maximum SERS enhancement given specified parameters.

A mathematical model using Mie scattering theory [13,14] was completed that allows for the calculation of the optimum nanoshell configuration for Raman enhancement given a substrate metal, excitation wavelength and Stokes shift. The calculation of the electromagnetic contribution to SERS using small gold colloid was previously described by Kerker et al [15]. This technique is expanded upon to calculate the electromagnetic Raman response of metal nanoshells. The primary modifications are the result of nanoshells being comparable in size to the wavelength of light. This method was first experimentally verified with silver nanoshells in an aqueous solution [12] as previously described.

The following calculation of the Raman response due to the local electromagnetic field follows work previously done by Kerker and Chew [15]. The field exciting the molecule E_ρ is taken as the sum of the incident plane wave E_{inc} and the local electromagnetic field E_{shell} on the nanoshell surface as calculated by Mie scattering theory [13]:

$$E_\rho(r',\omega_o) = E_{inc}(r',\omega_o) + E_{shell}(r',\omega_o)$$

The position of the molecule on the nanoshell surface is *r'*, the position of the observer is *r*, and the vector between *r* and *r'* is η. The incident frequency is ω_0 and the Stokes shifted frequency is ω. E_o is taken at the position of the molecule (*r'*) and at the incident frequency (ω_0). The excited molecule is treated as a dipole *p* oriented normal to the nanoshell surface, with a molecular polarizability, α:

$$\bar{p} = \bar{\bar{\alpha}} \cdot E_\rho(r',\omega_o)$$

which radiates at the Stokes frequency with electric field:

$$E_{dipole} = \frac{1}{\eta^3}\left[3\hat{\eta}(\hat{\eta}\cdot\bar{p}) - \bar{p}\right]$$

The molecular polarizability is taken as unity. The total Raman electromagnetic field at *r* is the sum of the electromagnetic field of the molecule's dipole and the shell response at the *Stokes shifted* frequency ω:

$$E_{Raman}(r,\omega) = E_{dipole}(r,\omega) + E_{shell}(r,\omega)$$

The electromagnetic field, E_{Raman}, is then calculated at r, for all r' on the nanoshell surface, assuming a monolayer of a molecule covering the surface of the nanoshell and allowing for a coverage of $0.3nm^2$ per molecule [16].

The following table illustrates the relative electromagnetic contribution to the Raman enhancement for various configurations of nanoshells using this model. The calculated electromagnetic Raman response as a function of metal (silver or gold), excitation wavelength (nm), Raman Mode (cm^{-1}), and surrounding medium (water or air). The core radius (nm) and shell thickness (nm) of the nanoshell that gives the maximum electromagnetic enhancement on an individual nanoshell are given

Substrate Metal	Excitation Wavelength	Stokes Mode	Medium	Core Radius	Shell Thick-ness	Theoretical Electromagnetic Contribution
silver	514	390	air	95	15	4.3493
silver	633	390	air	50	9	3.1866
silver	782	390	air	65	8	2.4512
gold	514	390	air	70	38	1.2867
gold	633	390	air	45	14	3.5162
gold	782	390	air	70	12	2.4708
silver	514	1077	air	45	14	29.5146
silver	633	1077	air	55	10	16.0217
silver	782	1077	air	70	8	9.8616
gold	514	1077	air	75	38	2.4913
gold	633	1077	air	50	15	18.4126
gold	782	1077	air	70	11	8.8881
silver	514	390	water	65	15	7.8866
silver	633	390	water	165	17	3.6911
silver	782	390	water	45	8	3.0438
gold	514	390	water	45	33	1.2738
gold	633	390	water	90	23	3.7354
gold	782	390	water	45	11	3.1014
silver	514	1077	water	70	16	79.3992
silver	633	1077	water	175	18	22.761
silver	782	1077	water	50	9	15.6246
gold	514	1077	water	45	38	5.2062
gold	633	1077	water	90	20	17.6156
gold	782	1077	water	45	11	14.0369

Table 1: Optimal nanoshell geometry for various surface enhanced Raman conditions.

Essentially, this calculation couples the electromagnetic response at the incident frequency to the electromagnetic response at the shifted frequency through the Raman polarizability tensor of the molecule. Until recently [17,18] the plasmon response at the shifted frequency was overlooked in the analysis of experimental SERS spectra. However, the coupling is not necessarily due to the molecule alone, rather it is more than likely attributable to the molecule-substrate complex, and therefore affected by any nonlinear responses of the substrate, such as photoluminescence [19]. These types of considerations are ignored here. The absolute magnitude of the Raman enhancement of a plasmonic system is not calculated; however this calculation allows for comparison of the electromagnetic Raman response of different plasmon resonant materials or, in this context, nanoshells with different silica core radii and metallic shell properties.

This calculation is purely electromagnetic in nature, chemical effects associated with molecular bonding of the analytes to the metallic surface are neglected. These types of considerations must be taken into account in choosing a particular nanoshell for a particular SERS system. For example, in **Table 1** it is clear that a silver nanoshell has a stronger Raman response when

working at an excitation wavelength of 514 nm. However, if the analyte has a stronger affinity for gold, or perhaps the analyte is in a biological environment (where there is a background level of autofluoresence in the visible spectrum), it may be more advantageous to use a gold nanoshell (which has a stronger Raman response in the near-infrared). Silver typically has a stronger plasmon resonance than gold, however in the core shell geometry the difference in the plasmon resonance at wavelengths greater than ~633 nm is minimal.

This calculation expresses the importance of the nanoshell plasmon resonance overlapping both the incident wavelength and the Stokes shifted wavelength. The typical nanoshell plasmon resonance line-width is such that the excitation wavelength and shifted wavelengths are easily accessible.

Results for Objective 1B – Use FDTD modeling to determine the optimum geometry of Nanoshells for maximum SERS enhancement given specified parameters.

A large amount of SERS investigations have focused on using aggregated colloid [1, Kneipp, 1997 #12]. The electromagnetic near field of a metallic aggregate is significantly increased compared to that of an isolated colloid [20]. Previous SERS investigations of silver nanoshells in solution showed that the finite absorption of nanoshells at the Raman emitted wavelength hampered the SERS signal enhancement. In order to maximize the Raman signal, the experimental geometry must be such that the reabsorbed light is a minimum, such as nanoshells immobilized on a surface. Controllable deposition of metallic colloids is challenging, and the investigation of such a geometry demands the investigation of the electromagnetic response of clusters of nanoshells. Mie scattering is limited in this regard, and finite methods must be employed.

The Finite-Difference Time-Domain (FDTD) method is an explicit time marching algorithm used to solve Maxwell's curl equations on a spatial grid. This method involves the propagation of the local electric and magnetic fields in real time. The specifics of the system to be studied enter the problem through the grid, the boundary conditions between different materials and through the local variation of the electric permittivities and magnetic permeabilities. In the case of nonlinear and dispersive materials, the electric and magnetic susceptibilities of various orders also enter. Although several codes are already available for FDTD calculations in general, we have found none suitable for the description of the optical properties of nanoparticles such as nanorods or nanoshells, assemblies of such nanoparticles, lithographically-patterned array structures, or local fields on vicinal molecules.

We have made substantial progress in the development of an efficient, 3D FDTD code for plasmonic nanostructures. The geometry for the simulation of a typical scattering problem (for the formulation of FDTD we have adopted) is shown in **Figure 1**. The target object is surrounded by a closed region where the incident wave is illuminated. The incident wave and target object interact, leading to a scattered wave that propagates outwards from the target object. The scattered wave travels outside of the interior region where the incident wave is illuminated. The scattered fields are then recorded on a virtual surface using discrete Fourier transforms, shown here as a blue dotted line. Finally, the scattered waves are attenuated away in an absorbing layer. These absorbing layers simulate the extension of the computational space to

infinity preventing any scattered waves would to be reflected back towards the target object, leading to unphysical results.

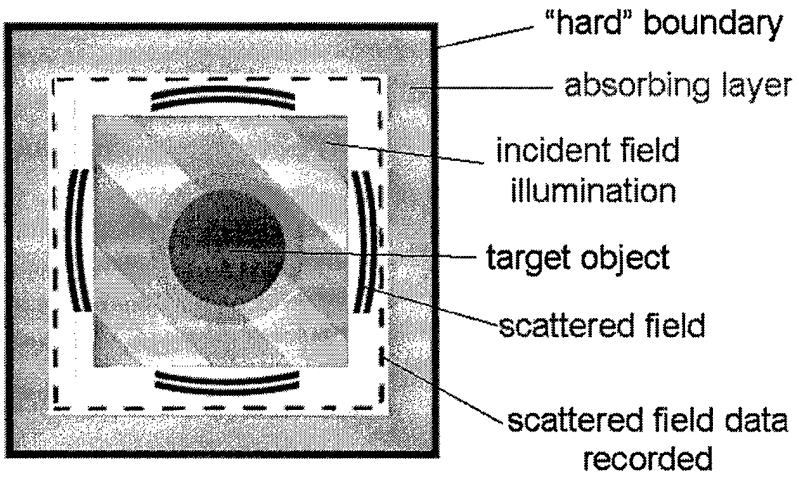

Figure 1. FDTD simulation geometry for a typical scattering problem. Our code allows the user to specify the size, shape, and material of the target object(s) and the nature of the incident excitation, which may be an arbitrary waveform with arbitrary incident direction and amplitude.

The sources of errors in the method are well known. Modeling new systems is reduced to grid generation, as opposed to deriving geometry specific equations. Thus, previously uninvestigated and potentially complex geometries do not require new formalisms. The time marching aspect of the method allows one to make direct observations of both near and far field values of the electromagnetic fields and at any time during the simulation. With these "snap shots" the time evolution of the electromagnetic fields can be measured and visualized. This opportunity provides new insight into the dynamics of the system under study. Additionally the FDTD method is easily parallelizable due to the local nature of finite differences. This localized aspect enables the use of simple parallel methods, such as domain decomposition, on either shared or distributed memory systems. Since FDTD uses the curl form of Maxwell's equations, the method is fully retarded.

To simulate the electromagnetic response of metals, a Drude dielectric function was fitted to a particular frequency range of the Johnson and Christy bulk dielectric data [21] for the metal under study.

$$\varepsilon = \varepsilon_\infty - \frac{\omega_p^2}{\omega^2 + i\omega\delta}.$$

For gold, the numbers we used were $\varepsilon_\infty = 9.5$, $\omega_p = 8.9488$ eV, and $\delta = 0.06909$ eV. For silver we used $\varepsilon_\infty = 5.0$, $\omega_p = 9.5$ eV, and $\delta = 0.0987$ eV. A comparison of our fitted Drude model to the bulk values for silver is shown in **Figure 2**.

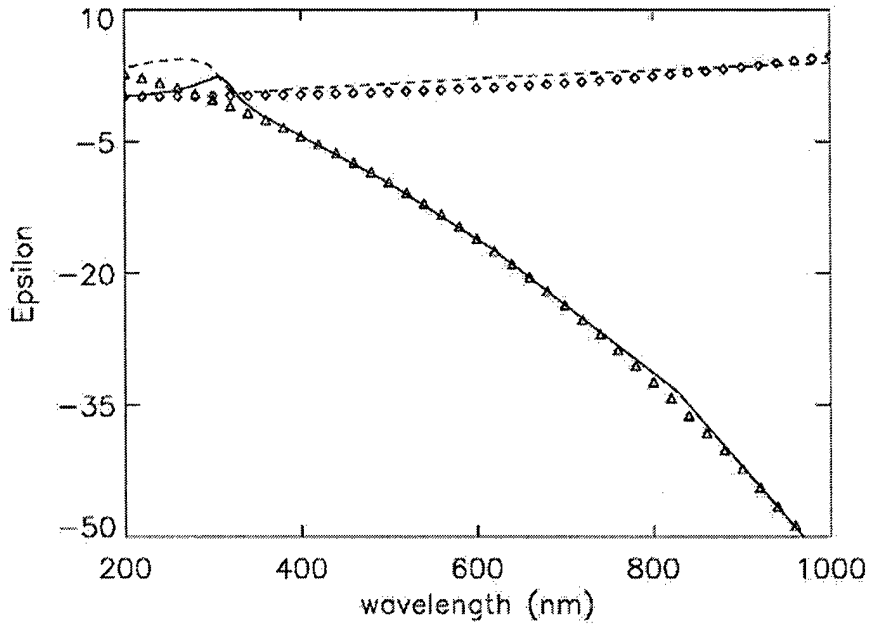

Figure 2. Comparison of the Johnson and Christy bulk dielectric data for silver [Weast, 1982 #43] (solid line is the real part and the dashed line is the imaginary part) and our Drude fit (triangles are the real part and diamonds are the imaginary part.

In order to estimate the numerical errors introduced in our implementation of the FDTD algorithms we investigate how the extinction cross section of a nanoshell depends on cell size. **Figure 3** is the calculated plasmon wavelength and peak height of a silver nanoshell as a function of mesh size. The nanoshell has a core radius of 39 nm and a 9 nm thick silver shell.

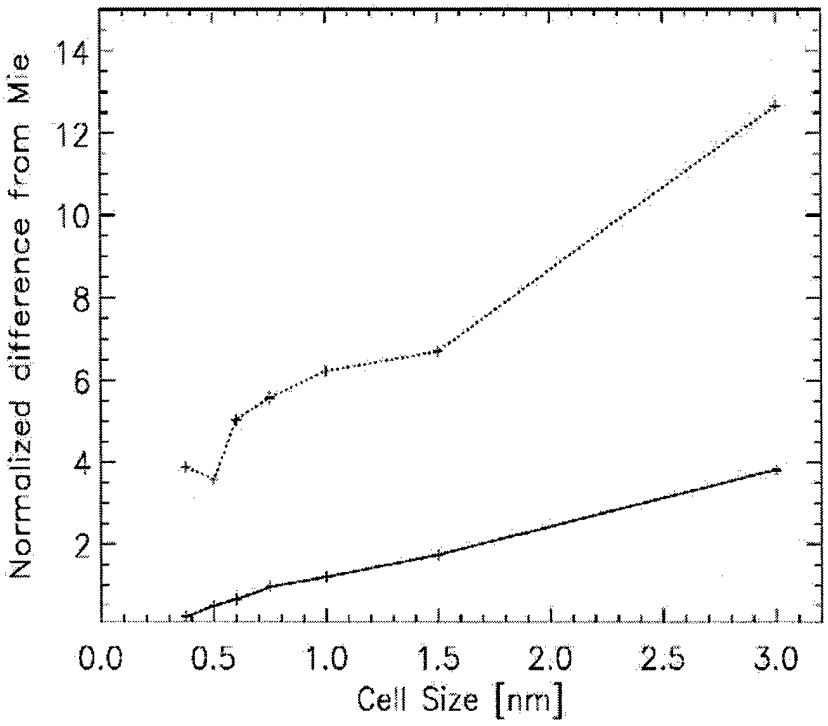

Figure 3. The normalized error, as a function of mesh size, for FDTD calculations of the dipole peak location (solid) and height (dotted) in the extinction cross section of a 39 nm radius silica core with a 9 nm thick silver shell. Results were compared to the classical Mie theory prediction. The last point was calculated with a larger Courant number and a smaller UPML separation to reduce runtime.

The electromagnetic enhancement at 718 nm of a nanoshell dimer consisting of two nanoshells each with a core radius of 39 nm and shell thickness of 9 nm, separated by 1.5 nm is shown in **Figure 4**. As expected, the largest electromagnetic response is located along the dimer axis between the nanoshells.

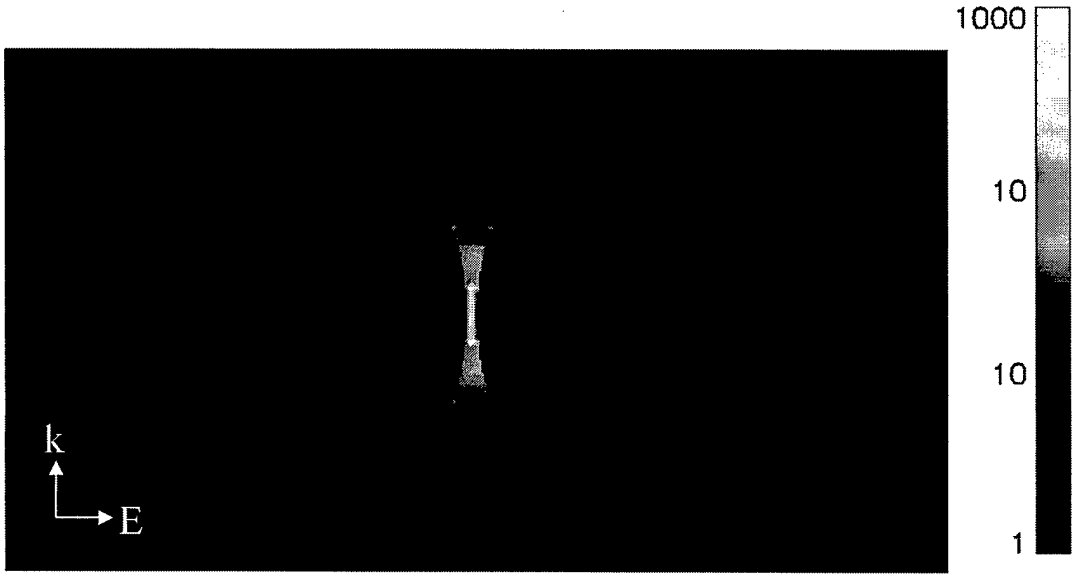

Figure 4. Near field enhancements for a nanoshell dimer consisting of two 39 nm radius cores with 9 nm silver shells and a separation 1.5 nm at a wavelength of 718 nm. The maximum electric field enhancement shown here is 250.

The electromagnetic Raman contribution is estimated by considering the fourth power of the electromagnetic enhancement. **Figure 5** is the sum of the fourth power of the electric field enhancements in a 2D slice along the axis of symmetry containing one of the nanoshells in a dimer, as a function of dimer separation. For large separations the sum is close to the single nanoshell result. At roughly a diameter separation there is a strong onset and the sum of E^4 grows exponentially. For the closest distances shown, the dimer enhancement is four orders of magnitude greater than the single nanoshell.

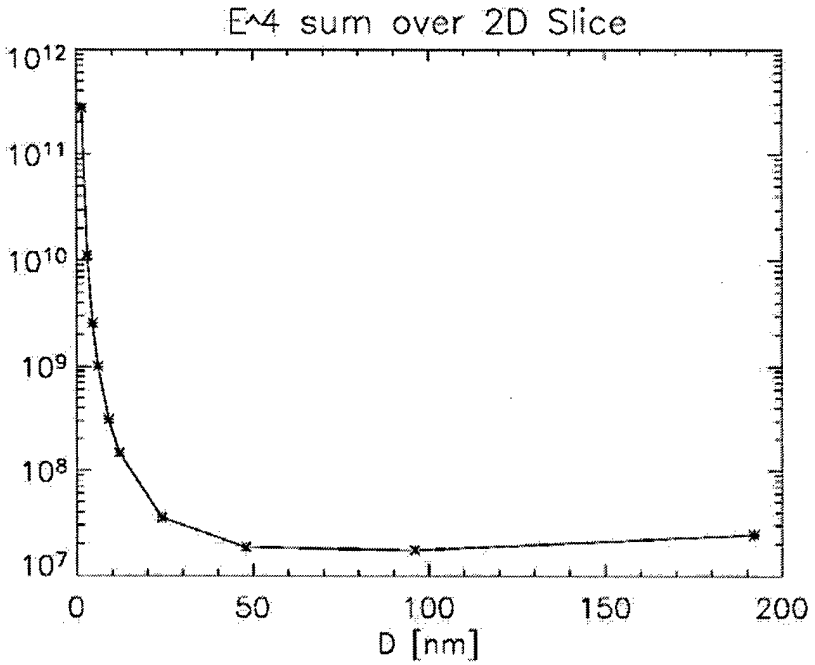

Figure 5. The sum of the fourth power of the electric field enhancements in a 2D slice along the axis of symmetry containing one of the nanoshells in a nanoshell dimer, as a function of dimer separation. The nanoshells consist of a 39 nm radius silica core and a 9 nm thick silver shell.

Figure 6 is a comparison the near field in the region of maximum enhancement as a function of wavelength for the single nanoshell and a nanoshell dimer of separation 1.5 nm. Also included in **Figure 6** is a scaled plot of the extinction cross section for the nanoshell dimer. The dimer enhancement is much larger than the single shell enhancement for all wavelengths shown. **Figure 6** also reveals a broad tail in the enhancement as compared to the far field extinction cross section spectra.

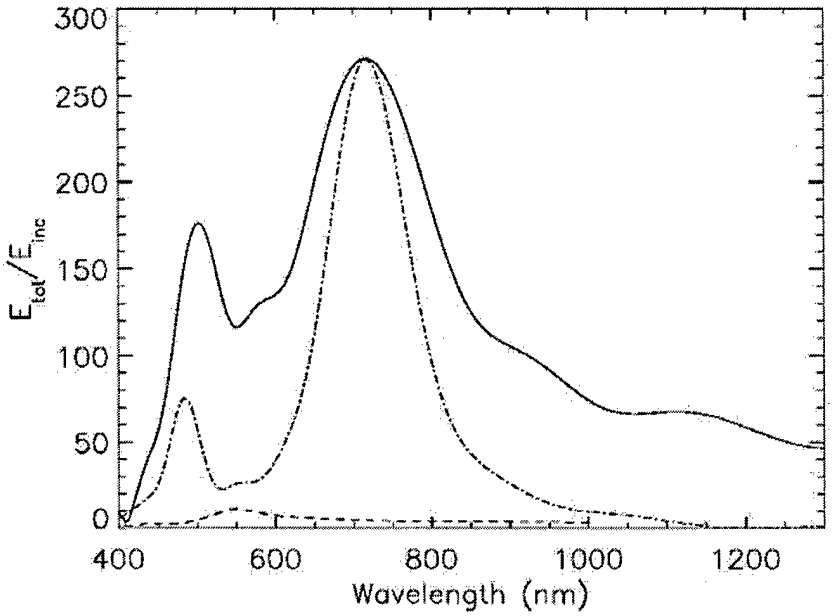

Figure 6. A plot of the near field in the region of maximum enhancement as a function of wavelength for a 39 nm radius silica core with a 9 nm silver shell (dashed) and a dimer made of the same nanoshell with a 1.5 nm separation (solid). Also included is a scaled plot of the extinction cross section for the nanoshell dimer (dash-dot)

Figure 7 and **Figure 8** are the near field enhancements of a gold nanoshell trimer at 604 nm and 752 nm, respectively. The nanoshells consist of a 55 nm radius core and a 16 nm thick gold shell. Notice the electromagnetic enhancement occurs at different junctions in the nanoshell trimer for different excitation wavelengths.

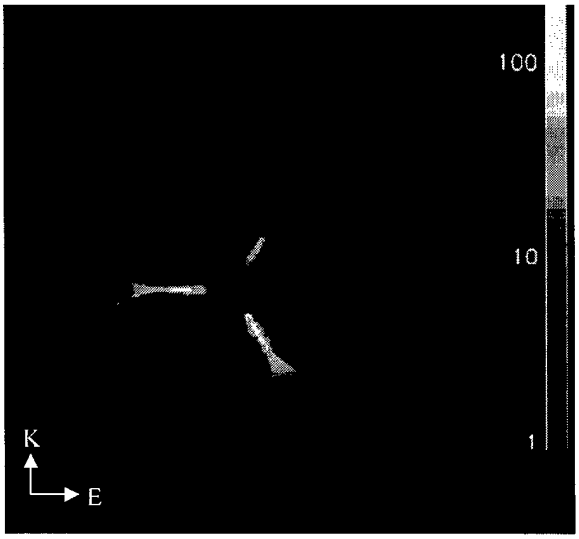

Figure 7. Near field enhancements for a 50 nm radius silica core with a 16 nm thick gold nanoshell trimer at a wavelength of 604 nm. Maximum electric field enhancement shown here is 200.

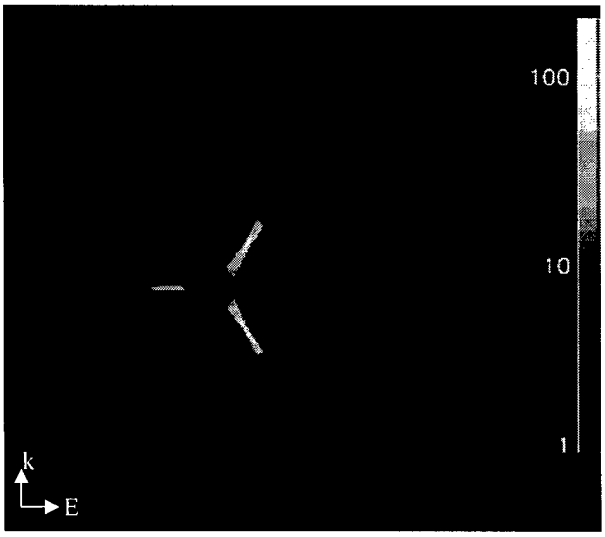

Figure 8. Near field enhancements for a 50 nm radius silica core with a 16 nm thick gold nanoshell trimer at a wavelength of 752 nm. Maximum electric field enhancement here is 150. Note the enhancement occurs in a different region from **Figure 7**.

This model would imply that aggregated nanoshells would provide enhancements greater than individual nanoshells. However, there are significant difficulties inherent in attempting the reproducible manufacturing of a substrate comprising such geometry. As a result, the remainder of our work was confined to construction and testing of individual nanoshell substrates, including the verification that the enhancements achieved were from individual nanoshells (and therefore reproducible) and not aggregates.

Objective 2 – Develop methods for manufacturing Nanoshell-based film substrates.

Previous studies of silver nanoshells in solution yielded Raman enhancements of mercaptoaniline on the order of 10^6- 10^8. As stated previously, the Raman scattering light is reabsorbed by other nanoshells in solution, hampering the measured Raman enhancement. This reabsorption is removed by immobilizing nanoshells on a planar surface. The deposition of nanoshells must be controlled in a manner as to investigate the individual nanoshell plasmon resonance contribution to the SERS, as well an any nanoshell-nanoshell interaction contribution to the SERS. Two methods for manufacturing nanoshell based film substrates were explored in detail throughout the course of these investigations: (i) dense nanoshell films deposited by vapor deposition and (ii) films with nanoshells anchored by a molecular linker to the slide.

Dense Nanoshell Films

Silica core-Ag nanoshell nanoparticles were constructed using 39 nm, 58 nm, 81 nm, and 94 nm radius silica cores, upon which silver layers ranging from 7 nm to 18 nm were deposited by a previously reported method [7]. Following fabrication, UV-Vis spectroscopy measurements were correlated with Mie scattering theory for each nanoshell sample to verify core diameter and shell thickness [7,8]. Comparison with theory showed that deviations in the shell thicknesses of ~1-2 nm were present in all nanoshell samples fabricated. The nanoshells were deposited into a film by evaporating 300μL aliquots of a nanoshell solution at ~10^8 particles/ml onto a 7 mm^2 area of a glass microscope slide until complete surface coverage is achieved. A representative optical micrograph of the dense nanoshell film is shown in **Figure 9**. The inset shows a TEM image of the nanoshells prior to deposition.

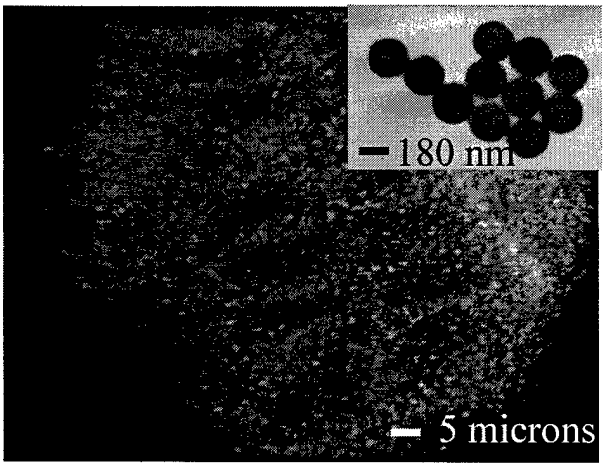

Figure 9. A representative optical micrograph of the dense nanoshell films after deposition onto the glass substrate and a TEM image of the nanoshells prior to deposition (inset).

This initial method of substrate preparation was chosen to normalize nanoshell surface area as the size of nanoshells was varied. In order to compare Raman signal from different core/shell configurations, the nanoshell surface area, and hence the same number of adsorbate molecules probed, would be held relatively constant by using these dense films for each Raman measurement. This allows for comparison to the theoretical simulations of the electromagnetic Raman response discussed in Objective 1A. The results of this comparison are discussed in Objective 3.

PVP/Nanoshell Films

In order to develop a substrate useful for aqueous samples, as well as to control the deposition of nanoshells on the substrate, we investigated methods of anchoring nanoshells to a glass substrate. We performed a literature search of methods of anchoring nanoparticles. Options considered from the literature included poly-4-vinylpyridine (PVP) [22], 3-amino-propyl-tri-ethoxy-silane (APTES), and cysteamine. We chose PVP as an anchoring molecule because of the molecule's robust nature. Further investigations into molecular anchors may be warranted as commercial products become developed.

Films of isolated nanoshells were deposited onto PVP-functionalized glass substrates [22]. Glass substrates were first cleaned in a piranha cleaning solution (70% sulfuric acid: 30% hydrogen peroxide). The substrates were then rinsed with milli-Q water and submerged in a 1% solution of PVP (100mg PVP/10mL ethanol) for 12 hours. The substrates were removed from the PVP solution, rinsed with ethanol, and submerged in a gold nanoshell solution. The gold nanoshells fabricated for these experiments had a core radius of 94 nm and a shell thickness of ~9 nm, as determined by comparing UV/Vis spectroscopy and Mie scattering theory. These nanoshell dimensions were chosen in order to exhibit a dipole resonance in air near the 782 nm Raman excitation wavelength. This was also independently verified by SEM during the nanoshell density analysis. The nanoshell deposition times of the substrates was varied from 15 minutes to 24 hours to obtain a variation in nanoshell density. To obtain the highest nanoshell densities, it was necessary to neutralize the surface charge of the nanoshells by the addition of 3mg of sodium chloride 12 hours into the deposition process.

An essential characteristic of a useable substrate is stability under different conditions. The PVP/nanoshell films were tested for stability by immersion in a strong acetic acidic solution, pH=1-2, and a strong ammonium hydroxide (basic) solution, pH=11-12. There was no detectable change in UV/Vis absorption or the Raman spectrum of adsorbed mercaptoaniline. In addition, there was no detectable change in the adsorbed mercaptoaniline SERS spectrum over a period of approximately two months. We elevated the temperature of the substrate to approximately 200°C, which is below the melting temperature of nanoshells [23] and the substrate remained stable. These substrates were also stable in highly saline solutions (1.2M) after the adsorbates are attached to the nanoshell. Salt will aggregate nanoshells in solution, as with metal nanoparticles [1], which will effect the deposition process, resulting in the deposition of large nanoshell aggregates.

Uniformity of deposition is a key condition for controlling variability of measured signals between slides. The PVP-nanoshell films were examined to determine the degree to which deposition could be controlled as well the degree to which aggregates were formed . Each nanoshell film was analyzed by taking at least 20 images at 2000X magnification and 10 images at 800X magnification. These images were analyzed by counting the number of nanoshells in an entire image area, tabulating the number of isolated nanoshells, the number of aggregates, and the number of nanoshells in each of the aggregates for each image area. Nearest neighbor considerations were ignored in this analysis; nanoshells were in an aggregate only if they appeared to be in contact with another nanoshell. In some larger aggregates it was necessary to estimate the number of nanoshells present by dividing the area of that aggregate by the area of a

single nanoshell. The probe area of the Raman instrument is a spot size of 2 μm; therefore all of the nanoshell densities are given as the number of nanoshells per spot.

A representative SEM image is given for several different nanoshell densities in **Figure10**. The area of the spot size is shown as the white circle.

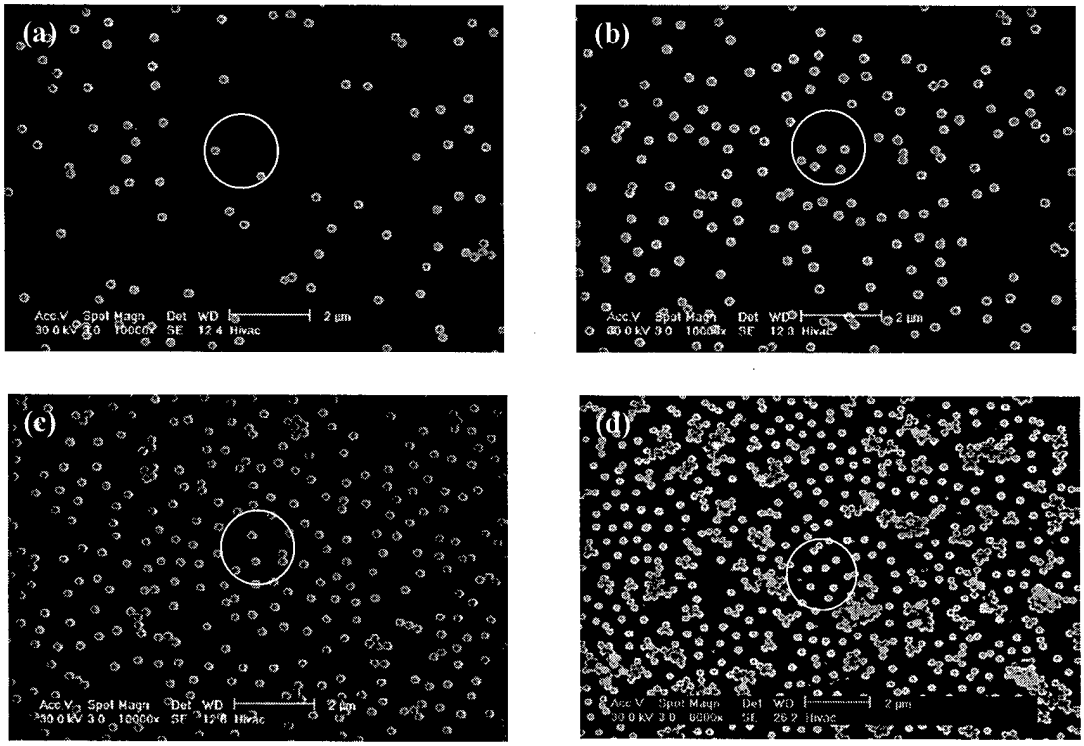

Figure 10. Representative SEM images of PVP/nanoshell films, characterized by the number of nanoshells per 2μm spot (NS/spot). The white circles in each image demonstrate the spot size. (a) 2.58±0.32 NS/spot, (b) 5.34±0.53 NS/spot, (c) 9.16±0.51 NS/spot, and (d) 16.66±1.9 NS/spot.

The characterization of these films is shown in **Table 2**. For completeness, the number of aggregates in each sample is demonstrated in two ways. First, the percentage of nanoshells in a cluster was found by taking the number of nanoshells in a cluster and dividing by the total number of nanoshells in all the images of that sample. This is the percent chance that a nanoshell probed in this sample was in an aggregate. Alternately, the percentage of particles that are clusters was found by taking the number of particles that are nanoshell aggregates and dividing by the total number of particles (the number of aggregates plus the number of free nanoshells). This is the percent chance that the laser is probing an aggregate during the Raman spectrum acquisition.

Average Number of Nanoshells/Spot	% of Nanoshells in Clusters	% of Particles That Are Clusters
2.58±0.32	29	14
5.34 ±0.53	25	12
9.16 ±0.51	21	14
12.12 ±1.7	47	39
16.66 ±1.9	59	46
15.75 ±2.1	72	53
32.15 ±4.9	87	83
complete coverage: 48.47		

Table 2. Nanoshell density analysis of the PVP/nanoshell films.

As a result of these experiments, we concluded that the deposition of nanoshells on the substrate could be controlled and that the substrates remained stable under a range of conditions (salinity, pH, temperature) that may be encountered in a commercial setting.

While PVP appears to be a suitable component for anchoring nanoshells on the substrate, other nanoshell preparation methods are currently being explored (i.e., amine terminated glass slides for nanoshell attachment) and may be considered in a Phase II application.

Air Force Objective 3 – Test Nanoshell-based film substrates for Raman enhancement.

Once nanoshell-based substrates had been manufactured and stability tested, our final objective was to measure Raman enhancement from the substrate. This work consisted of three steps:

(i) the verification of the Mie scattering model prepared in Objective 1A;
(ii) the calculation of Raman enhancements from silver nanoshells using a substrate prepared by vapor deposition;
(iii) as a measure of reproducibility, determining if enhancements were from single nanoshells or aggregates; and
(iv) the calculation of Raman enhancements from the PVP/gold nanoshell substrate.

Steps (i) and (ii) were performed using silver nanoshells directly deposited onto glass slides. Because of the inability to control deposition, step (iii) was performed using gold nanoshells anchored on substrates by PVP. Step (iv) concluded that the substrate developed provides significant enhancements as compared to other published studies.

Verification of the Mie Scattering Model from Objective 1A

For these experiments, *Para*-mercaptoaniline (pMA) was chosen as a target molecule given its well-established nonresonant Raman spectra [24]. pMA was deposited onto the nanoshell film by evaporating 10 μL of a 10 μM solution of pMA in ethanol. Raman spectra were obtained with a Renishaw micro-Raman spectrophotometer using a 782 nm excitation laser at 3.2mW power with a 2 μm spot size and 30 sec acquisition time. A typical stokes Raman spectrum of pMA adsorbed onto a nanoshell film is shown in **Figure 11(a)**.

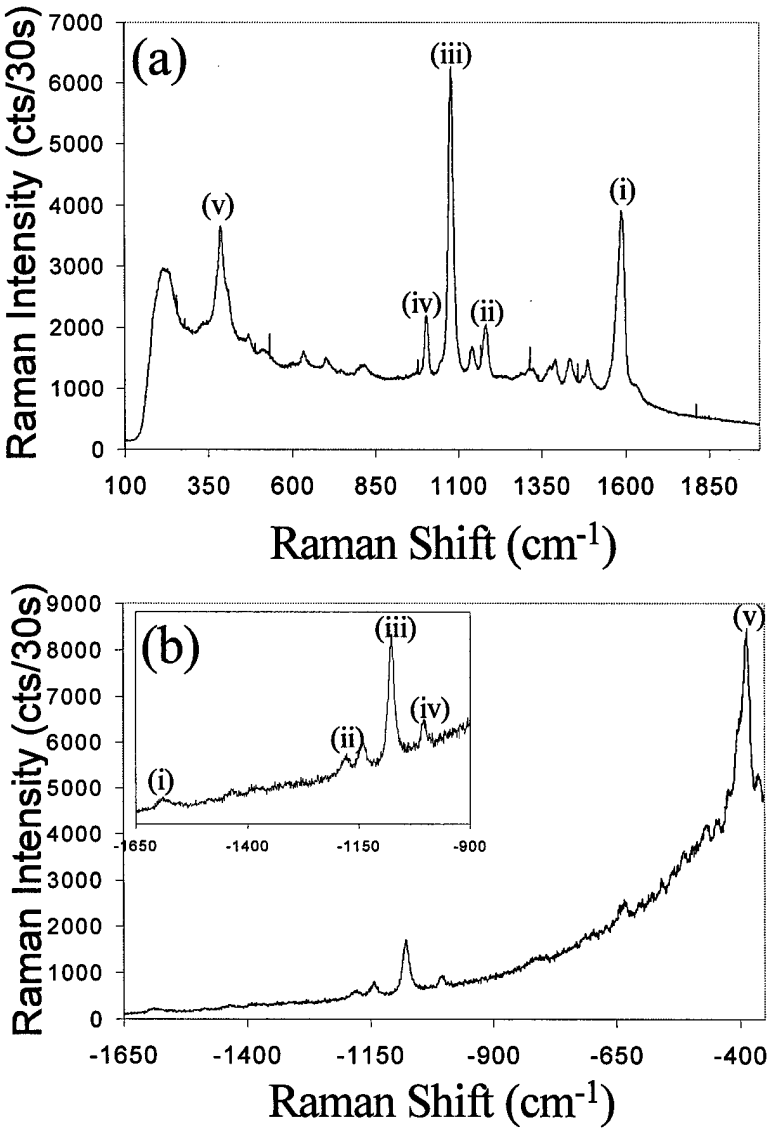

Figure 11. (a) Typical Raman spectra of nanoshells with adsorbed pMA in the dense film geometry. The arrows indicate the (i)1590cm^{-1}, (ii)1180cm^{-1}, (iii)1077cm^{-1}, (iv)1003cm^{-1}, and (v)390cm^{-1} ring vibrational modes of pMA that were examined as a function of nanoshell dimensions. (b) The corresponding anti-Stokes spectra.

The 1590 cm^{-1}, 1180 cm^{-1}, 1077 cm^{-1}, 1003 cm^{-1}, and 390 cm^{-1} ring modes of pMA are clearly observed in all spectra. It should be noted the Raman spectra obtained from these samples were stable over a period of at least 2 months.

To verify the Mie scattering model, the signal strength of each of these five modes was monitored as a function of silver shell thickness for various configurations of nanoshells (using four different silica core radii and various shell thicknesses). Anti-Stokes spectra were also obtained (**Figure 11(b)**) and the intensities of each Stokes mode was followed as a function of core and shell dimensions.

The results of the calculation of the electromagnetic contribution to the Raman effect, $|E_{Raman}|^4$, discussed in Objective 1A are shown as a function of core radius and shell thickness for the 1590 cm^{-1} and 390 cm^{-1} modes in **Figure 12**. This figure indicates the theoretical Raman response in air as a function of core radius and shell thickness for an excitation wavelength of 782 nm for these two modes (1590cm^{-1} and 390cm^{-1}). The stars in **Figure 12** represent the specific nanoshells fabricated for this experiment.

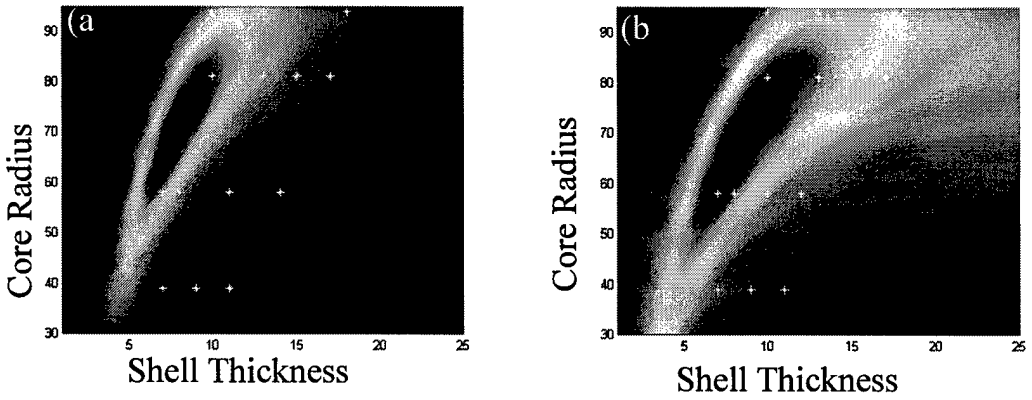

Figure 12. Calculated $|E_{Raman}|^4$ of (a) 1590cm^{-1} and (b) 390cm^{-1} modes as a function of core radius (nm) and shell thickness (nm). The white stars indicate the nanoshells fabricated for comparison.

The measured Raman spectra (peak height above background) are compared to the electromagnetic theory in **Figure 13**. For each mode, $|\mathbf{E}_{\mathbf{Raman}}|^4$ is plotted for a specific core radius as a function of shell thickness.

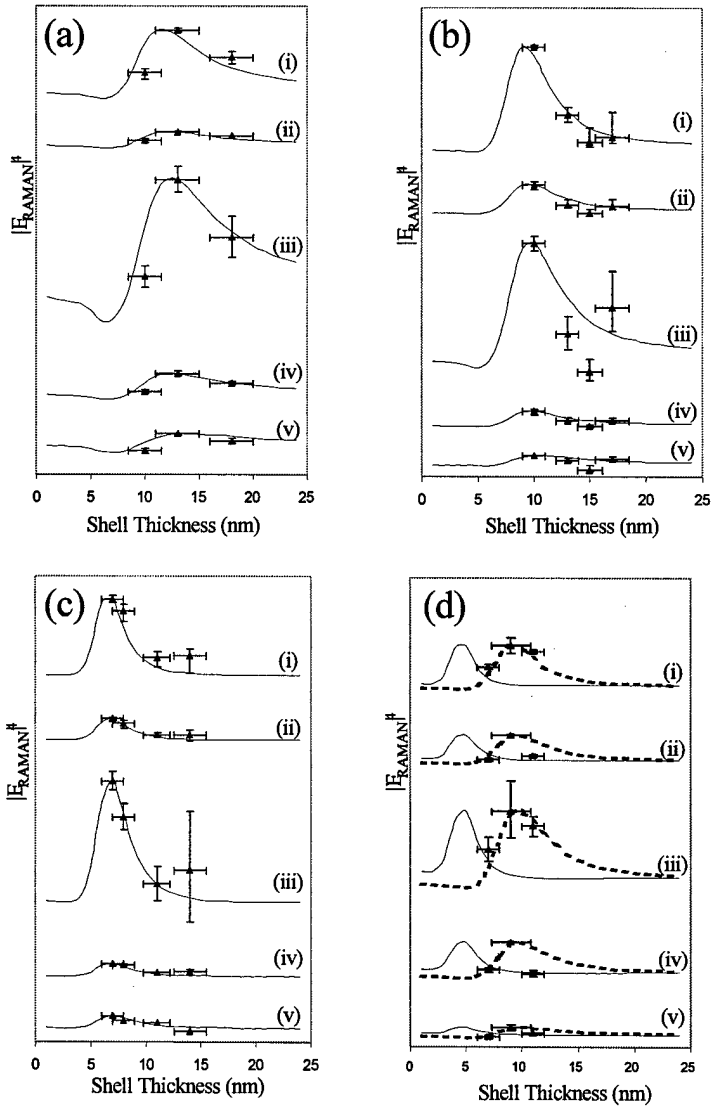

Figure 13. Results of comparison of the measured Raman modes to theoretical calculations. The normalized $|\mathbf{E}_{\mathbf{Raman}}|^4$ of the Stokes modes (i) 1590 cm^{-1}, (ii) 1180 cm^{-1}, (iii) 1077 cm^{-1}, (iv) 1003 cm^{-1}, and (v) 390 cm^{-1} are plotted for each fabricated core radius, where (a) 94 nm, (b) 81 nm, (c) 58 nm, and (d) 39 nm. The broken lines in (d) are an estimation of the first order aggregate Raman response (see text).

For comparison to measured values, $|\mathbf{E}_{\mathbf{Raman}}|^4$ is normalized to the maximum. The y-axis error bars arise from standard deviations between different nanoshell samples as well as different locations on the same sample. The x-axis error bars are the shell thickness deviations calculated from Mie scattering theory, assuming a Gaussian distribution in shell thickness. Excellent

agreement of the measured and calculated SERS response of nanoshells in **Figure 13(a), (b), and (c)** indicates that the SERS response follows the single nanoshell electromagnetic response in this geometry when the individual nanoshells are tuned near the excitation and Stokes frequencies.

The 39 nm radius core (**Figure 13(d)**) does not fit the single nanoshell response. However, we can deduce that the Raman response is due to the nearest neighbor resonance, or "dimer" resonance response. The dimer resonance is the resultant red shifted plasmon [25-27] of two nanoparticles in close proximity. For nanoshells, the dimer or aggregate resonance appears in the infrared, and was first experimentally observed by UV-Vis studies of infrared resonant nanoparticles [9]. The excitation wavelength and Stokes shifted wavelengths overlap spectrally closer to the estimated dimer resonance than with the single nanoshell plasmon. The dimer resonance can be estimated, to first order, by a single nanoshell with a core radius twice the size and same shell thickness. For example, the estimated dimer Raman response of a 39 nm radius core with a 9 nm thick shell would be the Raman response of a 78 nm (39x2) radius core with a 9 nm thick shell. In **Figure 14(b)**, we see that the 39 nm radius core points are detuned from the excitation/Stokes maximum, however, the estimated dimer resonance (78 nm radius core) is tuned near the excitation/Stokes maximum.

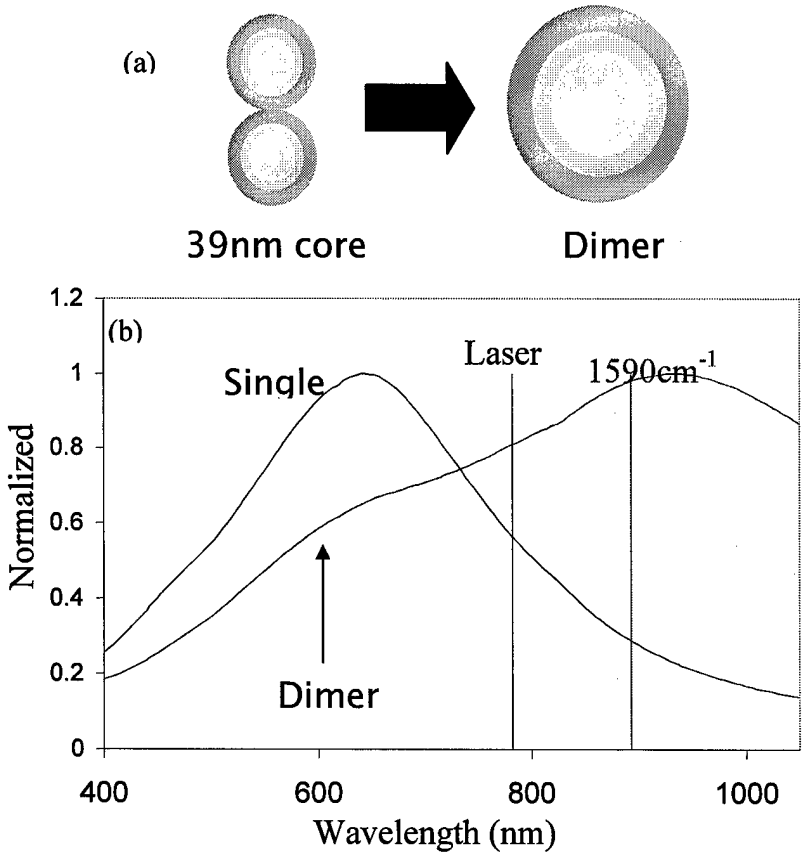

Figure 14. (a) Schematic of the first order aggregate response estimate used in **Figure 13(d).** (b) Calculated single nanoshell response of a 39 nm radius core with a 9 nm thick shell compared to the first order aggregate estimate, a nanoshell with a 78 nm radius core and 9 nm thick shell.

The Raman response of a 78 nm radius core is shown as the broken line in Figure 13(d). It can be deduced that the Raman response from the 39 nm radius core nanoshell film follows the inter-nanoshell plasmon or a nearest neighbor aggregate response.

Accordingly, we conclude that the Mie scattering model developed in Objective 1A provides a good predictor of optimum Raman enhancement and can be used for the selection of nanoshells for use with substrates for selected target molecules.

Calculation of Raman Enhancement

The silver nanoshell – vapor deposition substrates prepared as described in the previous section were utilized to calculate Raman enhancements to demonstrate that nanoshells in this geometry give reliable enhancements of a nonresonant molecule on the order of the greatest enhancements reported to date.

In order to compare with previously reported enhancements, the enhancement of nanoshells in this geometry is calculated using both a rate equation analysis, previously reported by Kneipp et. al. [1], and a comparison to reference method [17]. The Kneipp method investigates the measured value, K, of the anti-Stokes to Stokes ratio of the enhanced molecule with respect to the anti-Stokes to Stokes ratio of the molecule not enhanced.

$$K(\nu_m) = \frac{P_a^{SERS}(\nu_m)/P_s^{SERS}(\nu_m)}{P_a^{RS}(\nu_m)/P_s^{RS}(\nu_m)}$$

This is an instrument independent measurement of the deviation from the Boltzmann distribution, i.e. K=1 implies a Boltzmann distribution.

Using a two level steady state model, Kneipp estimates this value as:

$$K(\nu_m) = \sigma^{SERS}(\nu_m)\tau_1(\nu_m)e^{h\nu_m/kT}n_L + 1$$

where τ_1 is the lifetime of the first excited state (taken as10ps), n_L is the photon flux density (2.88×10^{23} photons/cm^{2}s), and σ^{SERS} is an effective Raman cross section. This equation assumes the Stokes and anti-Stokes cross sections are approximately equal and that $\sigma^{SERS}\tau_1 n_L \ll 1$. Although the validity of this approach has been questioned [28], it is the only method that reports actual measured enhancements without statistically guessing the number of molecules probed. This effective cross section is compared to a normal Raman cross section of 10^{-29} cm^2 to yield enhancement factors on the order of 10^{12}- 10^{15} for all core/shells/Raman modes measured. The enhancement from this rate equation analysis is averaged for each core radius, and the enhancement is plotted on a log axis as a function of Raman mode in **Figure 15(a)**.

Traditionally, the Raman enhancement is calculated [17] by assuming a linear relationship between the Raman intensity and the number of molecules probed. Using the reported packing density of the molecule (0.3 nm^2/molecule) [16] on a metal surface, the density of neat pMA (1.06 g/cm^3), and the optical setup parameters described previously, it is possible to estimate the

number of molecules probed in the enhanced and the non-enhanced samples ($1.05x10^6$ and $3.14x10^{15}$ molecules, respectively). The enhancement, G, is the weighted ratio of the measured Raman intensities of the enhanced signal vs. the non-enhanced signal described by:

$$G = \frac{RS^{ENH} * (\#\, molecules - ref)}{RS^{REF} * (\#\, molecules - sample)}$$

This yields enhancements on the order of 10^{10}-10^{12}. Using this method, the average enhancement for each core as a function of Raman mode is shown in **Figure 15(b)**. It should be noted here, these enhancement factors are consistent with the enhancement factors calculated for nanoshells in solution when reabsorption is taken into account [12].

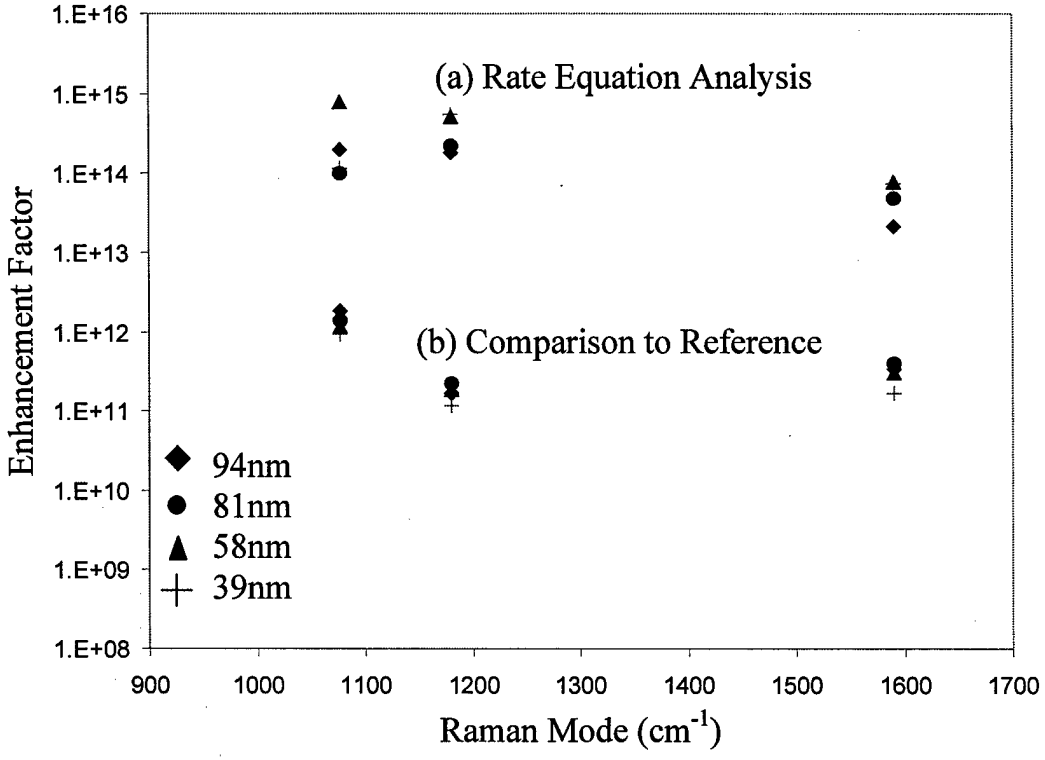

Figure 15. The average enhancement for the 94 nm (squares), 81 nm (circles), 58 nm (triangles), and 39 nm (crosses) radius cores as calculated by (a) a rate equation analysis (Kneipp method) and (b) a comparison to reference (traditionally).

It has been shown that when the nanoshell plasmon resonance is tuned near the excitation and Stokes shifted frequencies, the Raman response follows the single nanoshell response in a dense film geometry. This is radically different behavior than solid colloidal nanoparticles [29], where the Raman response is primarily due to nanoparticle aggregates. It was therefore necessary to analyze the Raman response arising from isolated nanoshells in a film geometry.

Verification Enhancements Are From Individual Nanoshells

In order to determine if the enhancements observed were from single nanoshells or aggregates, the PVP-anchored nanoshell films were utilized using varying densities of gold nanoshells as previously described.

The absorption (as measured by UV/Vis spectroscopy) of these PVP/gold nanoshell films is shown in **Figure 16**. As expected, the absorption increases as the nanoshell density increases.

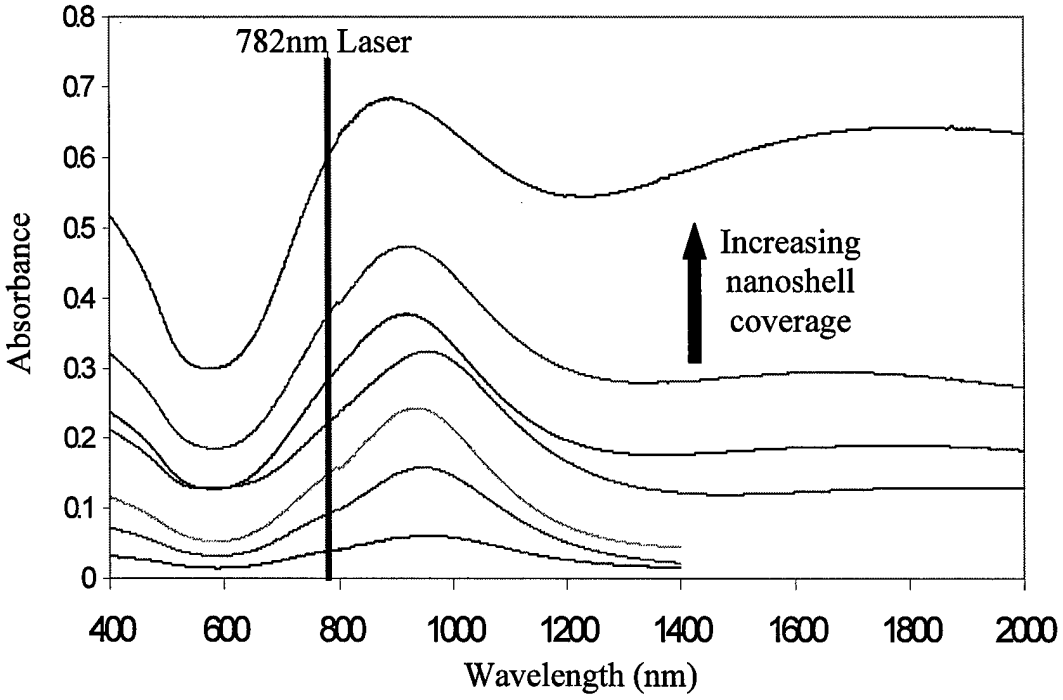

Figure 16. Absorption spectrum of the PVP/nanoshell films for each nanoshell density.

The isolated nanoshell plasmon resonance is represented by the peak at ~950 nm. The plasmon resonance of nanoshell aggregates becomes apparent at ~1800 nm as the nanoshell density increases. As stated previously, this nanoshell geometry was chosen to tune the single nanoshell plasmon resonance near the Raman excitation laser (782 nm), and de-tune from any aggregate resonances (which will be at wavelengths greater than 1300 nm).

The PVP/nanoshell films were submerged in a 100 μM solution of pMA for 3 hours to ensure saturation coverage of the available nanoshell surface. At least 30 Raman spectra, at random locations on each PVP/nanoshell film were taken. A representative Raman spectrum for each film is shown in **Figure 17**.

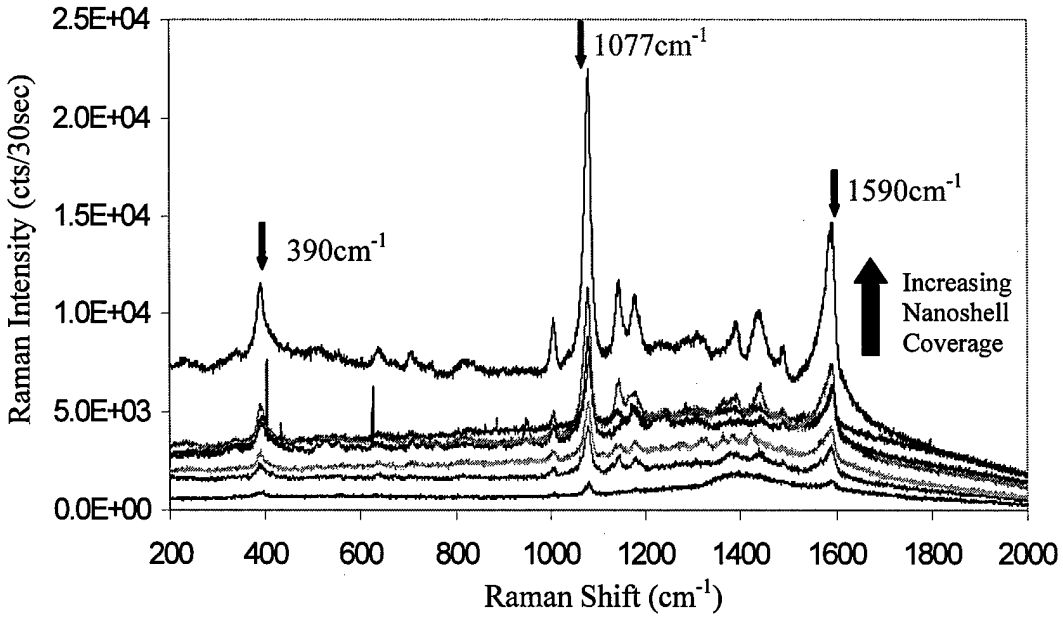

Figure 17. Representative Raman spectra of the PVP/nanoshell films for each nanoshell density.

The number of molecules probed increases with nanoshell density, so naturally the magnitude of the Raman response increases. It is interesting to note that the Raman baseline increases with nanoshell coverage as well.

Each Raman spectrum was analyzed as in the previous experiments. This analysis was confined to the 390 cm^{-1}, 1077 cm^{-1} and 1590 cm^{-1} modes because they were the only observable modes at the lowest nanoshell density. Magnitudes of these modes as a function of nanoshell density are shown in **Figure 18.**

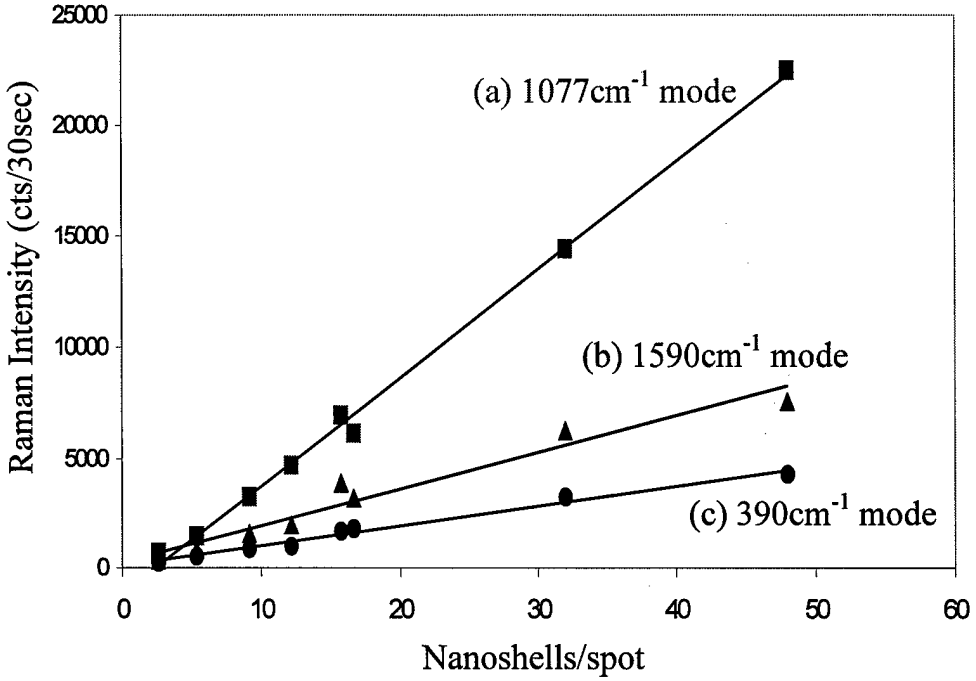

Figure 18. The (a) 1077 cm^{-1}, (b) 1590 cm^{-1}, and (c) 390 cm^{-1} Raman modes as a function of nanoshell density.

The standard deviation in the magnitudes of these Raman modes was ~25%. This error is due to the deviation of the number of nanoshells per spot shown in **Table 2.** The linear response of the Raman modes with nanoshell density confirms that the SERS response is from the single nanoshell resonance, not nanoshell-nanoshell interactions. The primary reason from this is the location of the single nanoshell plasmon resonance in relation to the excitation laser. The nanoshell-nanoshell interaction, or aggregate response, is detuned from the excitation laser and therefore does not contribute to the SERS response. It should also be noted here that the highest nanoshell density in **Figure 18** is not a PVP/nanoshell film but rather a dense nanoshell film.

This behavior is different than the Raman response of solid gold colloid. Zhu, et al. [29] conducted a similar experiment with various sizes of solid gold colloid, with an excitation wavelength of 632 nm, using the same Raman molecule pMA. In these experiments, there was a dramatic increase in the Raman response when the solid colloid particle density hit a threshold beyond which the particle-particle interaction dominated the Raman response. A dramatic increase was not seen in the nanoshell films, as indicated by the linear response in **Figure 18.**

Based on the linear results from these experiments, we conclude that the observed Raman enhancements are from individual nanoshells and not aggregates.

Raman Enhancement of PVP/Nanoshell Films

As previously described, we calculated significant enhancements from silver nanoshells deposited on dense films (see **Figure 14**). The PVP-gold nanoshell substrate is preferred because of the controllable deposition and stability in different media. Accordingly, we determined the relative enhancement from these substrates.

The Raman enhancement, G, is calculated using a weighted ratio as described previously.

$$G = \frac{RS^{ENH} * [reference]}{RS^{REF} * [sample]} \qquad (4)$$

The number of molecules in the sample, [sample], is estimated using the average number of nanoshells per spot, the surface area of the nanoshell, and the packing density of pMA [16]. This assumes that all of the nanoshell surface area contributes to the Raman response and therefore is a conservative estimate of the Raman enhancement. The results of this calculation are shown in **Figure 19**.

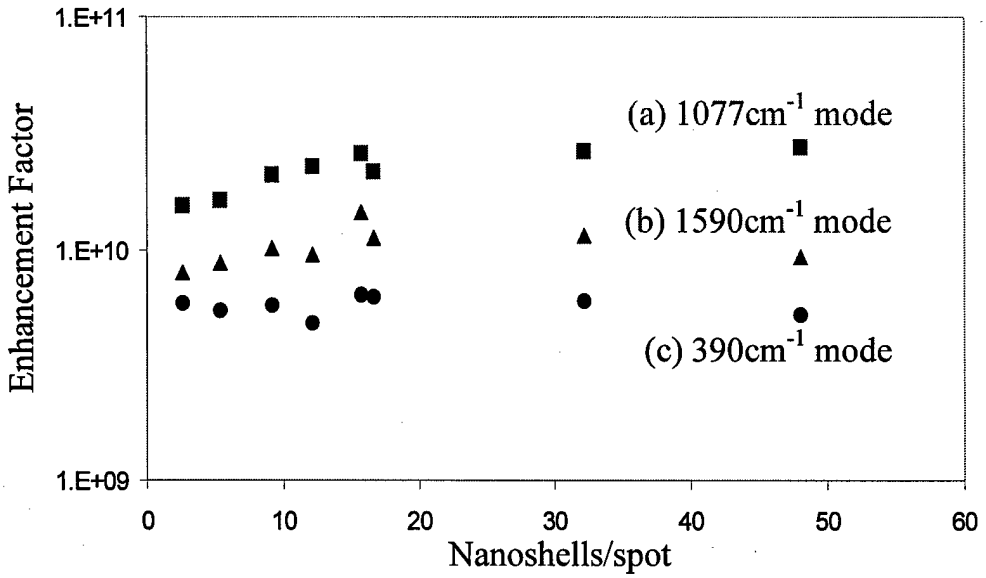

Figure 19. The Raman enhancement as a function of nanoshell density for the (a) 1077 cm^{-1}, (b) 1590 cm^{-1}, and (c) 390 cm^{-1} Raman modes.

The Raman enhancement is constant as function of nanoshell density. This emphasizes the idea of tuning to the single nanoshell and demonstrates that an isolated nanoshell can be used to achieve large Raman enhancements. Again, the largest nanoshell density in **Figure 19** is a not a PVP/nanoshell film but rather a dense nanoshell film. The enhancements of the PVP/nanoshell films are consistent with the Raman enhancements of nanoshells in solution (taking reabsorption into account) and nanoshells deposited in a dense film.

Detection Limits of Nanoshell Based Film Substrates

The enhancement factors reported in this document for the nonresonant molecule pMA are on the order of the highest reported enhancement factors to date [5,17]. It has been shown that previously reported single molecule detection enhancements factors of the resonant dye molecule rhodamine [5] can be achieved with the nonresonant molecule pMA using silver nanoshells. Single molecule detection is highly dependent on the molecular orientation of the molecule with the enhanced substrate and the field providing the enhancement.

The Raman response of serial dilutions of the adsorbate molecule pMA (below saturation coverage of the nanoshell surface) on PVP and dense nanoshell substrates were performed. Although Raman signals were obtained down to zepto-molar concentrations of pMA (statistically the single molecule limit), these results were inconsistent. Accordingly, these experiments should be repeated and further investigation into the molecular orientation of the molecule with respect to the nanoshell surface, as well as the position of the individual molecules on the nanoshell surface with respect to the excitation polarization, and effects such as "Raman blinking [5]" must be performed.

Conclusions

This research has demonstrated that nanoshells provide a robust substrate for the uniform enhancement of Raman signal, with an estimated enhancement exceeding 10^{10} from single nanoshells and is comparable to any other reports we have observed in the scientific literature. However, because this enhancement is not dependent on the geometry of the nanoshells (i.e., their proximity or arrangement of nanoshells in "hot spots" on the substrate), the nanoshell-based substrate has the advantages of being easy to manufacture and reproducible.

The Raman enhancement achieved from "individual nanoshell" substrates equals or exceeds 10^{10}, evaluated using direct comparison between the unenhanced and enhanced signal from the same molecule. It is important to note that when these enhancements are compared to those of Kneipp et al[1], who reported values of 10^{14}, the nanoshell-based enhancement appears to be approximately 10^{15} using their analytical method.

Accordingly, we believe this research demonstrates that nanoshells are a superior "optical method for the detection of species utilizing surface-enhanced Raman scattering" consistent with the Objective of this STTR Topic A03T003.

Phase II Opportunity

Based on this work, a Phase II program would pursue two principal objectives:

- Complete development and optimization of a nanoshell-based substrate. We will, as rapidly as possible, put this superior platform in the hands of other bio-defense researchers investigating molecular linkers for targets, developing Raman instrumentation, and developing bio-defense detection systems for chemical, viral and biological targets.

- Demonstrate that the nanoshell-based Raman detection system is applicable to a wide range of potential target molecules and biologicals. Rather than focus on developing a single or narrow targeting approach, our work will focus on applying a range of targeting molecules developed by others in collaboration with other researchers.

These two objectives will enable the pursuit of two possible commercialization strategies for nanoshell-based SERS substrates: supplying functionalized substrates for specific detection targets, or supplying unfunctionalized substrates along with specific functionalization protocols to assist the end user in development of a customized detection substrate for their specific use.

References Cited

1. K. Kneipp, Y. Wang, H. Kneipp *et al.*, *Phys. Rev. Lett.* **76**, 2444-2447 (1996).
2. M. Moskovits, *Rev. Mod. Phys.* **57**, 783 (1985).
3. R. R. Chance, A. Prock, and R. Silbey, *Adv. Chem. Phys.* **37**, 1-65 (1978).
4. D. L. Jeanmarie and R. P. Van Duyne, *J. Electroanal. Chem* **84**, 1 (1977).
5. K. Kneipp, Y. Wang, H. Kneipp *et al.*, *Phys. Rev. Lett.* **78**, 1667-1670 (1997).
6. Y. Y. Yu, S. S. Chang, C. L. Lee *et al.*, *J. Phys. Chem. B* **101**, 6661 (1997).
7. J. B. Jackson and N. J. Halas, *Journal of Physical Chemistry B* (2001).
8. S.J. Oldenburg, R. D. Averitt, S. L. Westcott *et al.*, *Chem. Phys. Lett.* **288**, 243-247 (1998).
9. S.J. Oldenburg, J. B. Jackson, S.L. Westcott *et al.*, *Appl. Phys. Lett.* **111**, 2897-2899 (1999).
10. S. J. Oldenburg, G. D. Hale, J. B. Jackson *et al.*, *Appl. Phys. Lett.* **75**, 1063-1065 (1999).
11. L. R. Hirsch, J. B. Jackson, A. Lee *et al.*, *Anal. Chem.* **75**, 2377 (2003).
12. J. B. Jackson, S. L. Westcott, L. R. Hirsch *et al.*, *Applied Physics Letters* **82**, 257 (2003).
13. G. Mie, *Annalen der Physik* **25**, 377-445 (1908).
14. A. L. Aden and M. Kerker, *J. App. Phys.* **22**, 1242 (1951).
15. M. Kerker, D. Wang, and H. Chew, *Appl. Opt.* **19**, 4159-4174 (1980).
16. N. Mohri, S. Matsushita, and M. Inoue, *Langmuir* **14**, 2343-2347 (1998).
17. C. L. Haynes and R. P. Van Duyne, *J. Phys. Chem. B* **107**, 7426-7433 (2003).
18. N. Felidj, J. Aubard, G. Levi *et al.*, *Appl. Phys. Lett.* **82**, 3095-3097 (2003).
19. M. R. Beversluis, A. Bouhelier, and L. Novotny, *Phys. Rev. B* **68**, 115433 (2003).
20. P. Nordlander, C. Oubre, E. Prodan *et al.*, *Nanoletters* **4**, 899-903 (2004).
21. R. C. Weast, "CRC Handbook of Chemistry and Physics; 63rd ed.," (CRC Press, Boca Raton, 1982).
22. S. Malynych, I. Luzinov, and G. Chumanov, *J. Phys. Chem. B* **106**, 1280-1285 (2002).
23. C. Radloff and N. J. Halas, *Applied Physics Letters* **79**, 674-676 (2001).
24. M. Osawa, N. Matsuda, K. Yoshii *et al.*, *J. Phys. Chem* **98**, 12702-12707 (1994).
25. K.-H. Su, Q.-H. Wei, X. Zhang *et al.*, *Nanoletters* **3**, 1087-1090 (2003).
26. W. Rechberger, A. Hohenau, A. Leitner *et al.*, *Optics Communications* **220**, 137-141 (2003).
27. G. Chumanov, K. Sokolov, and T. M. Cotton, *J. Phys. Chem.* **100**, 5166-5168 (1996).
28. T. L. Haslett, L. Tay, and M. Moskovits, *J. Chem. Phys.* **113**, 1641-1646 (2000).
29. Z. Zhu, T. Zhu, and Z. Liu, *Nanotechnology* **15**, 357-364 (2004).